2016 IEEE 55th Conference on Decision and Control (CDC)
ARIA Resort & Casino
December 12-14, 2016, Las Vegas, USA

Locomotive Analysis of a Single-Input Three-Link Snake Robot

Tony Dear[1], Scott David Kelly[2], Matthew Travers[1], and Howie Choset[1]

***Abstract*— When commanding gaits for snake robots and other articulated systems, direct control of all possible joint inputs may not always be necessary or optimal to achieve a locomotive goal. Here we consider a three-link nonholonomic snake robot—an already underactuated system with locomotive capabilities in $SE(2)$—and reduce its input space to a single actuated joint, replacing the other joint's motor with a passive mass-spring-damper system. We show that the modified system can operate dynamically in addition to kinematically, and that it is possible to find gaits that produces locomotion similar to a fully actuated system. In particular, we describe the emergence of a new type of gait that incorporates the system's singular configurations to produce high locomotive efficiency without incurring unbounded constraint forces.**

I. INTRODUCTION

Recent work in snake robotics has produced powerful tools to help with the design of gaits for desired locomotion. Oftentimes the robots' basic gaits, or segments of them, mimic "natural" behaviors in their biological counterparts or follow closely the passive dynamics that minimize the energy expenditure of the system. In this work, this led to the question, "Can such 'natural' gaits emerge on their own if we do not command the full input?"

Traditionally, simple slithering-like motions that propel a snake robot forward can be synthesized using *backbone curves* that constrain the large number of joints in the system, but in a simple and intuitive way that maintains full control over all degrees of freedom (DOFs) [1], [2]. However, because the number of DOFs is large, it is possible that some joints need not be actively controlled, and that the same or similar overall motions could be achieved by leaving some joints compliant. Matsuno and Mogi [3] describe how to make a wheeled snake robot "redundancy controllable" by selectively using wheel-free links, allowing for the control of multiple objectives, including inertial position and orientation as well as internal shape.

In this paper, we take one of the simplest examples of a snake robot and consider a three-link robot whose motion is governed by a nonholonomic constraint on each link (Fig. 1). Although this system appears to be less complex compared to a n-link snake, it actually has received attention from researchers treating it as a *kinematic* system [4]–[6], so named because its three constraints eliminate the need to consider second-order dynamics when modeling its locomotion. The mathematical structure of this system also lends itself to visualization and design tools [7]. Here we modify the system by making one of its two input joints compliant rather than actuated. We show how this system is still able to locomote using gaits not too different from those of the fully actuated system, and how one may consider system or gait design to achieve desired motion.

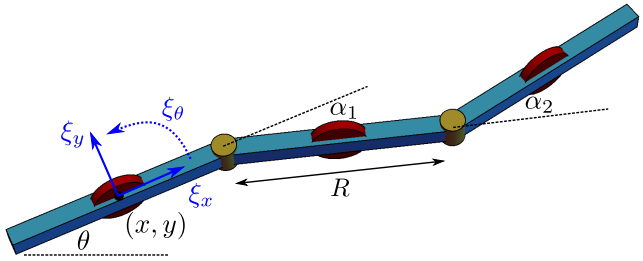

Fig. 1: A three-link nonholonomic robot. The coordinates (x, y, θ) describe the inertial position and orientation of the first link, which can also be described in a body-attached frame with velocities $(\xi_x, \xi_y, \xi_\theta)$. The joint angles (α_1, α_2) describe the relative configurations of the links thereafter.

We will also be able to exploit the modified system's singular configurations, which arise when the links are aligned such that the three constraints are no longer independent of each other. For a general system, singular states may entail the loss of a controlled DOF, so motion plans often actively avoid the straight or arc configurations in snake robots [8], [9]. A full analysis of the conditions for singular configurations in a n-link robot was done by Tanaka and Tanaka [10]. In preceding work on the three-link robot, we showed how to appropriately model the transitions between normal and singular system operation under a hybrid model, and we described how this may be achieved in a physical system with external forcing, as well as its novel locomotive capabilities [11]. Here we will show that attaching a spring to the passive joint can replicate this behavior without relying on external forces, allowing for dynamic motions.

The rest of this paper is organized as follows. Section II introduces the standard kinematic model of the nonholonomic snake system, how the system structure leads to visualization and design tools, and finally the dynamics of making one of the joints compliant rather than actuated. In Section III we first consider the simpler case of having a locked joint and allowing the system to maneuver itself into the singular configuration without having to rely on external forces. We then turn to full periodic input gaits in Section IV that give rise to locomotion in both familiar and novel ways, the latter also utilizing the system's singularities. We conclude

[1]T. Dear, M. Travers, and H. Choset are with the Robotics Institute at Carnegie Mellon University, Pittsburgh, PA 15213, USA. {tonydear@, mtravers@andrew., choset@cs.}cmu.edu

[2]S. D. Kelly is with the Department of Mechanical Engineering and Engineering Science at the University of North Carolina at Charlotte, Charlotte, NC 28223, USA. scott@kellyfish.net

in Section V with future directions and an example of how some of the preceding observations may be combined.

II. MECHANICAL MODEL OF THE SNAKE

A. Kinematics

As shown in Fig. 1, the three-link robot consists of three rigid links, each of length R, which can rotate relative to one another. Its configuration is defined by $q \in Q = G \times M$, where $g = (x, y, \theta)^T \in G = SE(2)$ specifies the position and orientation of the first link in an inertial frame; we measure a link's position at the center of the link. The joint angles $r = (\alpha_1, \alpha_2)^T \in M$ specify the links' relative orientation as shown. We can view Q as a principal fiber bundle, in which trajectories in the shape or base space M lift to trajectories in the group G [12].

The wheels at the centers of the links provide a set of nonholonomic constraints that restrict the system's motion. Each of the constraints can be written in the form

$$-\dot{x}_i \sin\theta_i + \dot{y}_i \cos\theta_i = 0, \tag{1}$$

where $(\dot{x}_i, \dot{y}_i)$ is the velocity and θ_i is the orientation of the ith link. These quantities can be found via the system's geometry and written in terms of the configuration coordinates and velocities. We note that the constraints are symmetric with respect to the group in that they do not explicitly depend on where the system is positioned or how it is oriented in space. We can ultimately rewrite the constraints into a reduced Pfaffian form [6] as

$$\omega_\xi(r)\xi + \omega_r(r)\dot{r} = 0, \tag{2}$$

where $\omega_\xi \in \mathbb{R}^{3\times3}$ and $\omega_r \in \mathbb{R}^{3\times2}$. The variables $\xi = (\xi_x, \xi_y, \xi_\theta)^T$ give us the body velocity of the system, as shown in Fig. 1. In $SE(2)$, the mapping that takes body velocities to inertial velocities is given by $\dot{g} = T_e L_g \xi$, where

$$T_e L_g = \begin{pmatrix} \cos\theta & -\sin\theta & 0 \\ \sin\theta & \cos\theta & 0 \\ 0 & 0 & 1 \end{pmatrix}. \tag{3}$$

Since the number of independent constraints is equal to the dimension of the group, these equations are sufficient to derive a kinematic connection for the system [6]. In other words, the constraint equations fully describe the first-order dynamics of the group variables in terms of the shape variables only. Thus, Eq. (2) can be rearranged to show this explicitly as the *kinematic reconstruction equation*:

$$\xi = -\underbrace{\frac{1}{D}\begin{pmatrix} \frac{R}{2}(\cos\alpha_1 + \cos(\alpha_1 - \alpha_2)) & \frac{R}{2}(1 + \cos\alpha_1) \\ 0 & 0 \\ \sin\alpha_1 + \sin(\alpha_1 - \alpha_2) & \sin\alpha_1 \end{pmatrix}}_{\mathbf{A}(r)} \dot{r}, \tag{4}$$

where $D = \sin\alpha_1 + \sin(\alpha_1 - \alpha_2) - \sin\alpha_2$. $\mathbf{A}(r)$ is called the local connection form, a mapping that depends only on the shape variables, in this case α_1 and α_2. Note that this quantity is not well defined when $\alpha_1 = \alpha_2$, which corresponds to the singular configuration of the system. Effectively, the rank of ω_ξ drops to 2 as one of the nonholonomic constraints becomes redundant given the other two at this point.

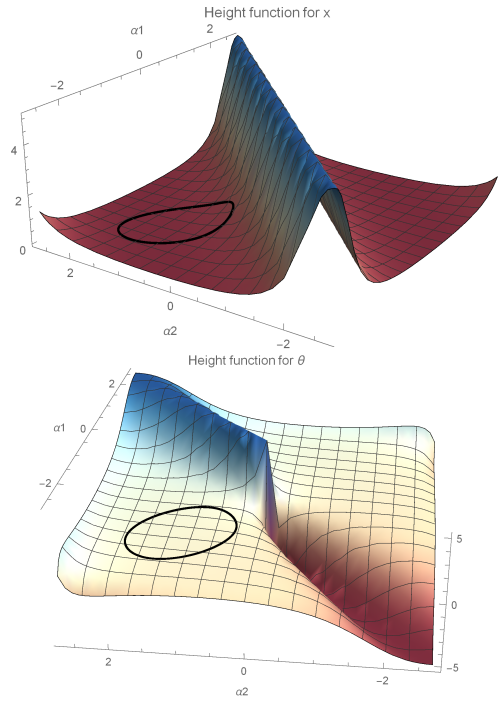

Fig. 2: Visualization of the connection curvature functions. Gaits can be represented as closed curves on the surfaces, while the enclosed volume (signed area) approximates displacement in each direction.

B. Joint Space Visualization

In the literature, the kinematic model (4) has yielded rich insights into the three-link system's locomotion. According to Hatton and Choset [7], Eq. (4) can be integrated over a gait γ to obtain a measure of displacement corresponding to the body frame directions. In the world frame, this measure provides the exact rotational displacement, *i.e.*, $\dot{\theta} = \xi_\theta$, and an approximation of the translational component, particularly for gaits of small magnitude.

By viewing each row of $\mathbf{A}(r)$ as a *connection vector field* and the gait γ as a closed trajectory on each of these fields, one can apply a change of variables along with Stokes' theorem to obtain

$$\int \mathbf{A}(r(t))\dot{r}(t)\,\mathrm{d}t = \int_\gamma \mathbf{A}(r)\,\mathrm{d}r = \iint_\Gamma \text{curl } \mathbf{A}(r)\,\mathrm{d}r. \tag{5}$$

Here, the integrand of the rightmost expression is the curvature of the local connection [6], [7], while Γ is the signed area of the portion of curl $\mathbf{A}(r)$ enclosed by γ.

The connection curvature functions allow us to easily visualize the effects of a gait over a cycle. Fig. 2 shows the x and θ curvature functions plotted as 2D surfaces, with the domain being various joint angle configurations and the surface height corresponding to the magnitude of curl $\mathbf{A}(r)$ (the y component is null everywhere).[1] The x curvature function is positive everywhere, meaning that any closed

[1] We follow [7] in plotting a scaled arctangent of the connection curvature function magnitudes in order to finitely show the singular portions. For the value x, we plot $\frac{1}{k}\arctan(kx)$ instead, where k is positive.

loop in joint space will lead to net displacement along the ξ_x direction, although the greatest volume occurs alongside the $\alpha_1 = \alpha_2$ singularity line. On the other hand, the θ function is symmetric about this line and anti-symmetric about $\alpha_1 = -\alpha_2$.

Since previous work traditionally assumed direct control over the joint angles or joint velocities, one can use these surfaces as a visual tool for gait design, parameterizing α_1 and α_2 (and their time derivatives) to achieve a desired motion. For example, one gait that moves the snake forward with minimal body rotation is represented by the black loop shown on the left side of the plots. Such a gait encloses a positive net volume on the x curvature function and zero net volume on the θ one, since it is symmetric about $\alpha_1 = -\alpha_2$.

C. Passive Joint Dynamics

We presently consider the case in which we assume control of only one of the joints, say α_1, and leave the other to be compliant, following the dynamics of a mass-spring-damper model. In doing so, we posit that full gaits can still merge from the natural dynamics of the modified system, allowing it to locomote efficiently with only one input. The modified system remains kinematic, as the nonholonomic constraints remain unchanged.

We use the Lagrangian formulation to derive the dynamics of the passive joint. As with the constraints, the energies are group-symmetric and do not depend on the position and orientation of the system. Denoting the global position of α_2 as (x_p, y_p), we have a kinetic energy

$$T(r, \xi, \dot{r}) = \frac{1}{2}\sum_{i=1}^{3}\left(m_i(\dot{x}_i^2 + y_i^2) + J_i\dot{\theta}_i^2\right) + \frac{1}{2}m_p(\dot{x}_p^2 + \dot{y}_p^2) \tag{6}$$

and a potential energy

$$U(r) = \frac{1}{2}k_p\alpha_2^2. \tag{7}$$

Here the quantities m_i and J_i are the masses and inertias of the respective links; m_p and k_p are the mass and spring constant of the passive joint. We can then define a reduced Lagrangian $l(r, \xi, \dot{r}) = T - U$, followed by a set of reduced Euler-Lagrange equations in the form

$$\frac{d}{dt}\left(\frac{\partial l}{\partial \xi^i}\right) = (\omega_\xi)_i^T\lambda, \tag{8}$$

$$\frac{d}{dt}\left(\frac{\partial l}{\partial \dot{\alpha}_2}\right) - \frac{\partial l}{\partial \alpha_2} = (\omega_r)_2^T\lambda - d_p\dot{\alpha}_2. \tag{9}$$

The object $(\omega_\xi)_i$ refers to the ith column of ω_ξ in Eq. (2) (and similarly for ω_r), while the Lagrange multipliers $\lambda \in \mathbb{R}^3$ represent the constraint forces. The constant d_p is a damping coefficient and the term $d_p\dot{\alpha}_2$ is appended to the α_2 Euler-Lagrange equation to capture the damping model component.

D. Singular Configuration Dynamics

While the relationship between the shape variables and the fiber variables remains kinematic despite the lack of control over one of the joints, this no longer remains true if the system is locked at a singular configuration in which

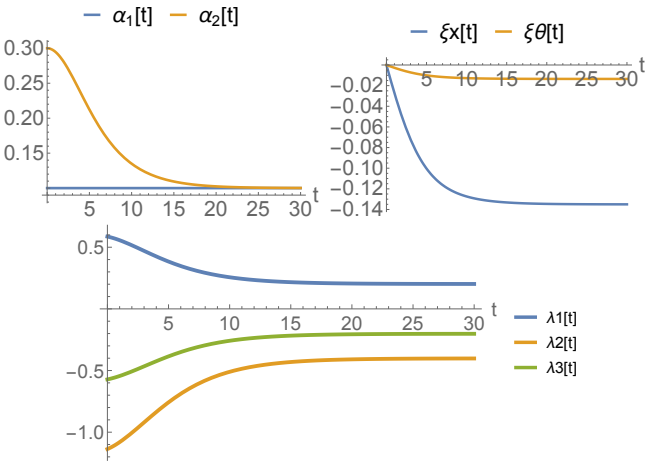

Fig. 3: The joint angle, body velocity, and constraint force trajectories for a system moving into the singular configuration $\alpha_1 = \alpha_2 = 0.1$.

$\alpha_1 = \alpha_2$. Starting the robot in a singular configuration with initial momentum will allow it to continue moving due to momentum conservation, even though the inputs $\dot{\alpha}_1 = \dot{\alpha}_2 = 0$. If we consider a hybrid model encompassing both the original kinematic and singular models as is done in [11], then this momentum can be defined so that the system's body velocities ξ vary smoothly between the two models.

The full details of the hybrid and transition modeling may be found in [11]. Consistency of the remaining two constraints requires that, in addition to $\xi_y = 0$, we have

$$\xi_x = \frac{R(1 + \cos\alpha)}{2\sin\alpha}\xi_\theta, \tag{10}$$

where $\alpha = \alpha_1 = \alpha_2$. This effectively describes a constant curvature trajectory on the plane. For α near 0, the robot travels along a path of small curvature, whereas the opposite true for α near $\frac{\pi}{2}$. If $\alpha = 0$, then all three links are aligned in the same direction. So the system would only be able to move along the ξ_x axis, while ξ_θ is necessarily 0.

III. LOCKED-JOINT LOCOMOTION

In our earlier work [11], we had noted that although a motion planner utilizing the singular configuration provides a novel way of locomotion, it was not intuitive how one would maneuver into this state in the first place. With two actuated joints, one option would be to directly command both joints to achieve a common angle α, but a problem arises in which the Lagrange constraint forces become unbounded. Alternatively, one can use an asymptotic command in which $\dot{\alpha}_1$ and $\dot{\alpha}_2$ both go to 0 as the configuration is approached, but this would lead to trivial behavior in which $\xi = 0$. We thus considered external forcing, for example in the form of gravity, alongside locking the actuated joint, which would "push" the system into the singular configuration while simultaneously giving it nonzero momentum to start moving. Here we will show that having a system with a passive spring-loaded joint can lead to the same result without relying on the external environment.

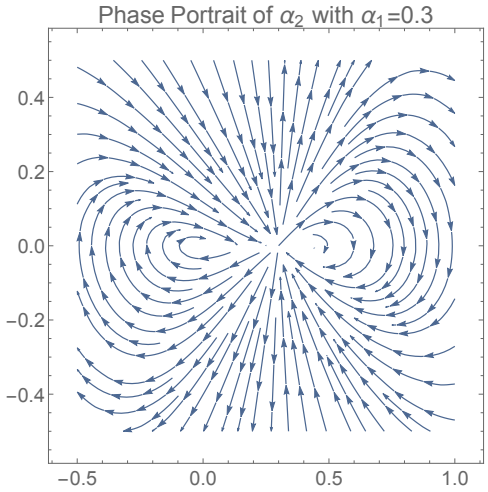

Fig. 4: The phase portrait for the α_2 dynamical system with α_1 constant. There is a stable fixed point at the origin and an unstable one at the singular configuration $\alpha_2 = \alpha_1$.

The spring restoring force plays the same effective role as the external force in "pushing" the compliant joint toward α, the locked value of α_1, while the rigidity of the nonholonomic constraint force prevents it from overshooting that value. If the system starts from rest, this can be achieved as long as $|\alpha_2(0)| > |\alpha_1|$. Fig. 3 shows the results of a simulation starting from rest with all parameters set to a value of 1. Because $\alpha_2(0) = 0.3$, its spring starts restoring it toward 0, but it reaches $\alpha = 0.1$ and is kept there by the nonzero but finite constraint forces acting on all three links. At the same time, the system starts moving and continues to do so with nonzero ξ after α_2 effectively reaches 0.1.

A phase analysis of α_2 yields a more general response to different initial conditions, as well as the stability of the singular configuration. From the reduced form of Eqs. (8), it is possible to analytically solve for the Lagrange multipliers and substitute them into Eq. (9). In addition, because Eq. (4) gives us the body velocities ξ in terms of the joint angles r and velocities $\dot{r}$, we can substitute them out to obtain a second-order differential equation in the shape variables, *i.e.*,

$$\ddot{\alpha}_2 = f(\alpha_2, \dot{\alpha}_2, \alpha_1, \dot{\alpha}_1, \ddot{\alpha}_1). \tag{11}$$

For a constant α_1, Eq. (11) becomes an autonomous dynamical system. The analytical expression for f is rather tedious to insert into this paper, but we can examine an example phase portrait of this system (Fig. 4). Again, the system parameters have all been set to 1, and $\alpha_1 = 0.3$. First we note the existence of a stable fixed point at $(0, 0)$, corresponding to the minimum spring potential configuration.

There is also a fixed point at $(\alpha, 0)$ corresponding to the singular configuration, which confirms the converging behavior observed in the simulation. Unlike the origin, it appears to be a saddle point with four distinct regions around it. Flows starting in the regions $(\alpha_2 > \alpha, \dot{\alpha} \leq 0)$ and $(\alpha_2 < \alpha, \dot{\alpha}_2 \gg 0)$ converge toward it, while those in the other regions diverge away. The physical interpretation of the first convergence region is due to the balance between the spring and constraint forces on α_2.

The mechanism behind the second region is due to the interplay between the constraint forces and the nonholonomic constraints themselves. As α_2 increases toward α, constraint forces become large enough to slow $\dot{\alpha}_2$ toward 0. At the same time, near $\alpha_1 = \alpha_2$ it can be shown that the constraints require $\dot{\alpha}_1 \approx -\dot{\alpha}_2$. Since $\dot{\alpha}_1 = 0$, $\dot{\alpha}_2$ will also tend toward 0 as α_2 approaches α_1, allowing it to stay there.

The divergence regions can be understood more easily. In both of them, the system starts with an initial velocity headed away from the singular configuration and is naturally pushed away by the nonholonomic constraint forces, with the latter effect being greater the closer α_2 is to α. This divergence is possible as long as the system has some nonzero velocity, despite the presence of damping and lack of active input. Eventually, these constraint forces become small enough that the restoring spring force takes over and pulls the joint back toward either 0 or α. This lack of stability may be troublesome for a physical system, but this could be alleviated by implementations such as a compliant motor system that can be locked when desired.

Proposition 1: Analytically, we can obtain these conclusions with the following Lyapunov function for Eq. (11):

$$V(\alpha_2, \dot{\alpha}_2) = \frac{1}{2}(\alpha_2 - \alpha)^2 + \frac{1}{2}\dot{\alpha}_2^2,$$
$$\dot{V}(\alpha_2, \dot{\alpha}_2) = (\ddot{\alpha}_2 + \alpha_2 - \alpha)\dot{\alpha}_2. \tag{12}$$

From the condition that $\dot{V} < 0$ for the stable regions near $\alpha_2 = \alpha$, one can derive a relationship among the parameters, in particular the spring and damping coefficients k_p and d_p. In the region $\alpha_2 < \alpha$, this gives the minimum velocity that $\dot{\alpha}_2$ must take in order for the joint to converge toward the singular configuration before being pulled back to the spring's resting state or damped out by friction.

IV. SINGLE-INPUT OSCILLATORY GAITS

Given what we know about the system's behavior with a constant α_1, we now consider continuously commanding α_1 with a periodic input $\alpha_1(t) = A_0 + A\cos(\omega t + \phi)$. We discuss two distinct simulation results that illustrate some of the possible behaviors that emerge. For both cases we set all masses and inertias, including m_p, to 1.

A. Non-Singular Configuration Gaits

In the first scenario, we command the joint trajectory $\alpha_1(t) = 0.5 + 0.3\cos t$. Assigning this joint some offset away from 0 is standard in the gaits in [6], [7], since this allows for a sufficient range of motion for both joints in hand-designed gaits without worrying about hitting the singular configuration. The initial value for α_2 is -0.4 and the passive joint parameters are $k_p = 1$, $d_p = 5$.

The values chosen above illustrate the mechanism behind resultant gaits like that in Fig. 5. In the steady state, α_2 tends to oscillate about the origin due to the spring restoring force, but not symmetrically. Because d_p is much higher than k_p, the combination of dissipation and the increasing constraint forces as α_1 and α_2 approach each other is large enough to

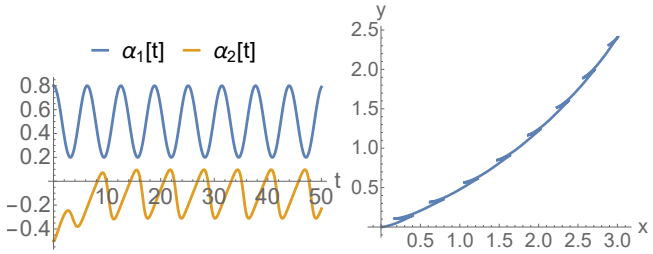

Fig. 5: Joint and workspace trajectories for a gait that does not cross the singular configurations.

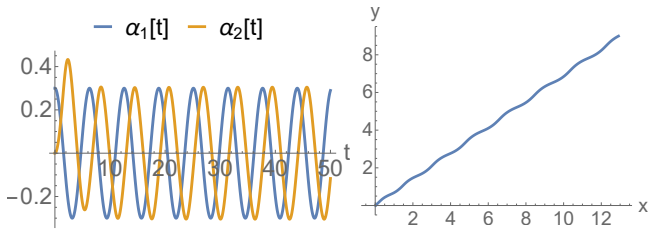

Fig. 6: Joint and workspace trajectories for a gait that periodically crosses the singular configuration.

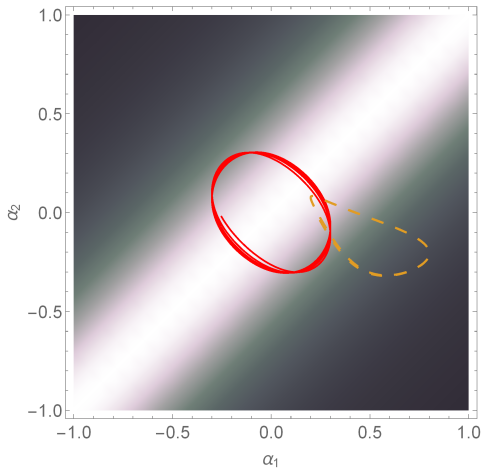

Fig. 7: Two gaits shown on a density plot of the x connection curvature function. The dashed brown gait does not cross a singularity configuration and encloses less area than the solid red, resulting in a lower locomotive displacement.

stop α_2 before α_1 reaches its minimum. At the maximum of α_2, the spring and constraint forces push α_2 back toward the origin, thus giving rise to a periodic gait.

More importantly, this gait leads to nontrivial locomotion in the workspace, and is similar to hand-designed gaits in that it can be represented on the corresponding connection curvature functions, shown as the dashed potato-shaped loop in Fig. 7. From a design perspective, the relative impedance of the passive joint due to the mass, spring, and damping values determine a tradeoff between gait amplitudes and the location in the joint space. A higher damping value allows for α_1 and α_2 to oscillate nearer each other, placing the gait closer to the high-volume, singular configurations to achieve greater displacement. However, this will also reduce the amplitude of α_2, leading to a narrow elliptical loop that encloses less area than a more circular, equal-amplitude gait would. We expect to further explore the design principles behind these models in future work.

B. Singular Configuration Gaits

Opposite to the case described previously, we now consider system parameters where d_p is smaller relative to k_p or initial conditions where α_2 starts off much closer to the α_1 trajectory. An example of both of these changes is shown in Fig. 6, where $\alpha_1(t) = 0.3\cos t$, and $k_p = d_p = 2$. The trajectory has the characteristics of a gait observed by Matsuno and Mogi [3] for redundancy controllable snake robots, in which crawling snakes naturally operated around the singular configuration; the authors sought to avoid this configuration due to potential loss of control. Here we will utilize it using phase analysis of the now time-dependent autonomous system. Plugging in α_1 and its derivatives into Eq. (11), f will still depend on t, but we can sweep over a complete gait cycle and observe that the high-level phase portrait structure remains unchanged. A "snapshot" at $t = 19.3$, at which $\alpha_1 = \alpha_2 = 0.27$, is shown in Fig. 8.

Because α_2 lags α_1 in the steady state, the passive joint is in an asymptotically stable region of the phase space at almost all times, allowing it to track α_1 (again, this observation is made not with the single phase portrait of Fig. 8, but rather with a sampling of portraits over a sweep of a gait cycle). Note that α_1 and α_2 are allowed to periodically cross each other. This is captured in the phase portrait by the existence of a clockwise flow line around the current singularity position at $\alpha_2 = 0.27$. Such a gait would have been very unintuitive to design even for a fully actuated system, as this single flow is the only trajectory that passes through without the constraint forces becoming unbounded. That the constraint forces become exceedingly large is characterized by the abrupt change in flow direction everywhere else along $\alpha_2 = 0.27$.

The fact that the resultant gait tracks so close to the singular configuration is desirable from a locomotive efficiency standpoint. We overlay this gait on the x connection curvature function as the red loop in Fig. 7 and see that much of it encircles a high volume region (lightly colored as opposed to dark). This corresponds to a much larger forward displacement compared to the previous emergent gait or any hand-designed gaits that are restricted to half of the joint space to avoid the singularities. Directly comparing Figs. 5 and 6 shows that for an input of equal amplitude in α_1, the latter is able to locomote about four times more in absolute displacement. Furthermore, because this particular gait is symmetric about the $\alpha_1 = -\alpha_2$ axis, it encloses minimal net volume on the θ connection curvature function (Fig. 2). This then leads to minimal net rotation over the course of the gait, allowing the system to effectively move in a straight line as shown in Fig. 6. This could be useful if movement only in a certain direction is desired, for example.

One can potentially combine the different gaits explored

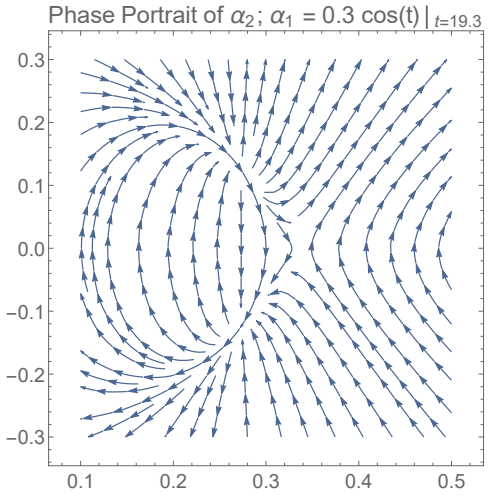

Fig. 8: The phase portrait for the α_2 dynamical system with $\alpha_1 = 0.3\cos t$ and $t = 19.3$. Unlike before, a flow line exists around the singular configuration $\alpha_2 = \alpha_1$.

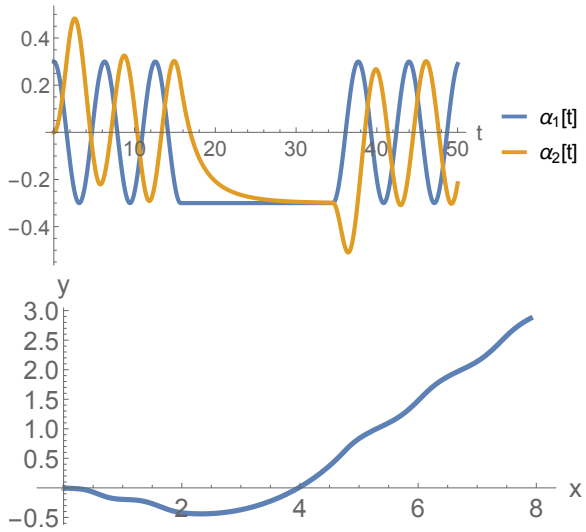

Fig. 9: A trajectory that combines the forward gait with the dynamic rolling gait for reorientation, potentially allowing the system to cover $SE(2)$ with only one controlled input.

to order to produce more flexible and complex trajectories. An example motion plan is shown in Fig. 9, where we stitch together two singularity-crossing gaits with a locked joint maneuver between them. The first and third parts of the motion plan effectively allow the system to move forward, as we recall that net reorientation is zero or minimal with a gait symmetric about $\alpha_2 = 0$. The intermediate part pins the system on a trajectory with constant known curvature, so this can be used to achieve a rotational transition when desired. By combining individual trajectories like these in different ways, the robot can travel between any two neighborhoods in $SE(2)$, a significant result as we are only controlling one degree of freedom at any given time.

V. CONCLUSIONS AND FUTURE WORK

In this paper we have considered the idea of reducing the locomotive effort necessary to achieve certain gaits or motions by allowing the system's passive dynamics to generate them instead. We presented an example in which this is viable in the form of a single-input, three-link snake robot and observed that a diverse set of gaits can still arise despite the loss of a degree of freedom. In particular, not only is the system still able to locomote, but it has also been shown to cross the singularity configurations, which lead to new rolling motions as well as high locomotive efficiency.

Looking forward, the nuances of the nonlinear system governing the evolution of the passive joint offer a way to design gaits for the actuated joint, just as with the fully actuated system in previous work. In particular, how do the relationships between the joint impedance parameters and the commanded gait determine whether a gait will encircle the singular configuration or not? More rigorous stability analyses, for both the locked joint and oscillatory input cases, can also yield information about the types of gaits that are useful over long runs. Finally, we would like to extend this work to snake robots with $n > 3$ links, where the actuation cost savings could be impactful.

REFERENCES

[1] G. S. Chirikjian and J. W. Burdick, "A modal approach to hyper-redundant manipulator kinematics," *IEEE Transactions on Robotics and Automation*, vol. 10, no. 3, pp. 343–354, Jun 1994.

[2] M. Tesch, K. Lipkin, I. Brown, R. Hatton, A. Peck, J. Rembisz, and H. Choset, "Parameterized and scripted gaits for modular snake robots," *Advanced Robotics*, vol. 23, no. 9, pp. 1131–1158, 2009.

[3] F. Matsuno and K. Mogi, "Redundancy controllable system and control of snake robots based on kinematic model," in *Decision and Control, 2000. Proceedings of the 39th IEEE Conference on*, vol. 5, 2000, pp. 4791–4796 vol.5.

[4] J. Ostrowski and J. Burdick, "Gait kinematics for a serpentine robot," in *Robotics and Automation, 1996. Proceedings., 1996 IEEE International Conference on*, vol. 2, Apr 1996, pp. 1294–1299 vol.2.

[5] J. Ostrowski, "Computing reduced equations for robotic systems with constraints and symmetries," *Robotics and Automation, IEEE Transactions on*, vol. 15, no. 1, pp. 111–123, Feb 1999.

[6] E. A. Shammas, H. Choset, and A. A. Rizzi, "Geometric motion planning analysis for two classes of underactuated mechanical systems," *The International Journal of Robotics Research*, vol. 26, no. 10, pp. 1043–1073, 2007.

[7] R. L. Hatton and H. Choset, "Geometric motion planning: The local connection, stokes theorem, and the importance of coordinate choice," *The International Journal of Robotics Research*, vol. 30, no. 8, pp. 988–1014, 2011.

[8] C. Ye, S. Ma, B. Li, and Y. Wang, "Locomotion control of a novel snake-like robot," in *Intelligent Robots and Systems, 2004. (IROS 2004). Proceedings. 2004 IEEE/RSJ International Conference on*, vol. 1, Sept 2004, pp. 925–930 vol.1.

[9] F. Matsuno and H. Sato, "Trajectory tracking control of snake robots based on dynamic model," in *Robotics and Automation, 2005. ICRA 2005. Proceedings of the 2005 IEEE International Conference on*, April 2005, pp. 3029–3034.

[10] M. Tanaka and K. Tanaka, "Singularity analysis of a snake robot and an articulated mobile robot with unconstrained links," *IEEE Transactions on Control Systems Technology*, vol. PP, no. 99, pp. 1–12, 2016.

[11] T. Dear, S. D. Kelly, M. Travers, and H. Choset, "The three-link nonholonomic snake as a hybrid kinodynamic system," in *American Control Conference(ACC), 2016*, To appear.

[12] S. D. Kelly and R. M. Murray, "Geometric phases and robotic locomotion," *Journal of Robotic Systems*, vol. 12, no. 6, pp. 417–431, 1995.